MITSUBISHI ELECTRIC RESEARCH LABORATORIES
http://www.merl.com

Nonlinearity-tolerant four-dimensional 2A8PSK family for 5-7 bits/symbol spectral efficiency

Kojima, K.; Yoshida, T.; Koike-Akino, T.; Millar, D.S.; Parsons, K.; Arlunno, V.

TR2017-038 February 2017

Abstract

We describe in detail the recently proposed fourdimensional modulation format family based on 2-ary amplitude 8-ary phase-shift keying (2A8PSK), supporting spectral efficiencies of 5, 6, and 7 bits/symbol. These formats nicely fill the spectral efficiency gap between dual-polarization quadrature PSK (DP-QPSK) and DP 16-ary quadrature-amplitude modulation (DP-16QAM), with excellent linear and nonlinear performance. Since these modulation formats just use different parity bit expressions in the same constellation, similar digital signal processing can be seamlessly used for different spectral efficiency. A series of nonlinear transmission simulation results shows that this modulation format family outperforms the conventional modulation formats at the corresponding spectral efficiency. We also investigate the adaptive equalizer for these modulation formats.

IEEE Journal of Lightwave Technology

Nonlinearity-tolerant four-dimensional 2A8PSK family for 5–7 bits/symbol spectral efficiency

Keisuke Kojima, *Senior Member, IEEE, Fellow, OSA,* Tsuyoshi Yoshida, *Member, IEEE, Member, OSA,* Toshiaki Koike-Akino, *Senior Member, IEEE, Member, OSA,* David S. Millar, *Member, IEEE, Member, OSA,* Kieran Parsons, *Senior Member, IEEE, Member, OSA,* Milutin Pajovic, *Member, IEEE,* and Valeria Arlunno, *Member, IEEE*

(Invited Paper)

***Abstract*—We describe in detail the recently proposed four-dimensional modulation format family based on 2-ary amplitude 8-ary phase-shift keying (2A8PSK), supporting spectral efficiencies of 5, 6, and 7 bits/symbol. These formats nicely fill the spectral efficiency gap between dual-polarization quadrature PSK (DP-QPSK) and DP 16-ary quadrature-amplitude modulation (DP-16QAM), with excellent linear and nonlinear performance. Since these modulation formats just use different parity bit expressions in the same constellation, similar digital signal processing can be seamlessly used for different spectral efficiency. A series of nonlinear transmission simulation results shows that this modulation format family outperforms the conventional modulation formats at the corresponding spectral efficiency. We also investigate the adaptive equalizer for these modulation formats.**

***Index Terms*—high-dimensional modulation format, adaptive modulation and coding, spectral efficiency, nonlinearity tolerance.**

I. Introduction

THERE is an increasing interest in flexible networks where adaptive transceivers select from multiple data rates, modulation formats, and forward error correction (FEC) overheads for efficient network usage [1]–[4]. For example, it has been shown that the mean loss in throughput per transceiver for a granularity of 100 Gb/s is four times larger than for a granularity of 25 Gb/s [4]. In order to cover wide range of channel conditions, multiple modulation formats with different spectral efficiency have been extensively studied [5]–[15].

Dual polarization (DP)-quadrature phase-shift keying (QPSK), star-8 quadrature-amplitude modulation (QAM), and 16QAM are widely used for 4, 6, and 8 bits/symbol transmission. Here we use bits/symbol defined in four-dimensional (4D) space of DP signaling. It has been recognized that DP-Star-8QAM does not always perform best for 6 bits/symbol, and many formats have been investigated [16]–[20]. In particular, 4D-2A8PSK has been shown to be superior to many other formats in linear and nonlinear performance, due to its large Euclidean distance, 4D constant modulus (constant power) characteristics, and Gray labeling [21]–[23]. In order to relate this to the block coding approach described in the context of high-dimensional modulation [11], 5, 6, and 7 bits/symbol modulation formats were introduced as a family of block-coded 2A8PSK in a unified manner in [24].

In this paper, we first review the family of 5, 6, and 7 bits/symbol modulation formats. We then conduct transmission simulations in a nonlinear dispersion-managed (DM) link, as well as a dispersion-uncompensated link, to verify that this proposed modulation family indeed shows excellent linear and nonlinear transmission characteristics. Through an analysis using separated nonlinear components, we also reveal that reduction of self-phase modulation (SPM) and cross-phase modulation (XPM) are the primary beneficial factors of the 4D constant modulus property. We next discuss several items related to practical implementations in a digital signal processor (DSP), which need some attention since the constellation is different from that of the conventional QAM-based formats. Finally we show that the penalty caused by practical DSP is small and the benefits far exceed the penalties. This paper provides additional contributions over the previous report [24]; more specifically, new detailed analyses (i.e., impact of DM, non-DM links, separated nonlinearity, and DSP algorithms) and improved modulation parameters (i.e., optimized block coding, set partitioning, ring ratio, and power ratio).

II. Modulation Formats

A. Generalized Mutual Information (GMI)

Conventionally, pre-FEC bit error ratio (BER) has been used to predict post-FEC BER performance of hard decision (HD) FEC systems. However, pre-FEC BER cannot be directly applied to modern optical communications systems, which rely on soft-decision (SD) FEC coding based on bit-interleaved coded modulation (BICM). As an alternative performance measure applicable for SD-FEC systems, the BICM limit, called generalized mutual information (GMI), has been recently introduced to the optical research community for comparing multiple modulation formats [25], [26]. Several modulation formats were compared using this metric [18],

Manuscript received October 30, 2016.

K. Kojima, T. Koike-Akino, D. S. Millar, K. Parsons, M. Pajovic, and V. Arlunno are with Mitsubishi Electric Research Laboratories (MERL), 201 Broadway, Cambridge, MA 02139, USA (e-mail: kojima@merl.com; koike@merl.com; millar@merl.com; parsons@merl.com; pajovic@merl.com; arlunno@merl.com). V. Arlunno is currently with Acacia Communications, 3 Mill and Main Place, Maynard, MA 01754, USA.

T. Yoshida is with Department of Microtechnology and Nanoscience, Chalmers University of Technology, SE-412 96 Gothenburg, Sweden, on leave from Information Technology R&D Center (ITC), Mitsubishi Electric Corporation (MELCO), 5-1-1, Ofuna, Kamakura, Kanagawa 247-8501, Japan (e-mail: Yoshida.Tsuyoshi@ah.MitsubishiElectric.co.jp).

[27]. The normalized GMI can be obtained from the log-likelihood ratio (LLR) outputs of the demodulator at the receiver as follows [28]–[30]:

$$I = 1 - \mathbb{E}_{L,b}\left[\log_2\left(1+\exp\left((-1)^{b+1}L\right)\right)\right], \quad (1)$$

where b, L, and $\mathbb{E}[\cdot]$ denote the transmitted bit $b \in \{0,1\}$, the corresponding LLR value, and an expectation (i.e., ensemble average over all LLR outputs L and transmitted bits b), respectively. We denote "normalized" GMI as the mutual information per modulation bit, not per modulation symbol. The normalized GMI can thus determine the maximum possible code rate of SD-FEC coding for BICM systems. Accordingly, multiplying the number of bits per symbol with the normalized GMI is equal to the achievable throughput per symbol.

In Fig. 1, we show the relationship between Q-factor calculated from pre-FEC BER and normalized GMI of four different modulation formats, i.e., DP-QPSK, DP-Star-8QAM, 6b4D-2A8PSK, and DP-16QAM. We will explain the 6b4D-2A8PSK modulation format in detail in Section II-D. Here, the Q-factor is defined by

$$Q^2_{\mathrm{BER}} = 2\cdot\{\mathrm{erfc}^{-1}(2\cdot \mathrm{BER})\}^2, \quad (2)$$

which is a classical measure to calculate the required signal-to-noise ratio (SNR) to achieve the BER for binary-input additive white Gaussian noise (AWGN) channels. Here, $\mathrm{erfc}^{-1}(\cdot)$ denotes an inverse complementary error function. From Fig. 1, it can be seen that the identical pre-FEC BER (Q-factor) does not achieve the same BICM limit for different modulation formats, in particular at lower code rate regimes. At the normalized GMI of 0.85, the Q-factor ranges from 4.77 dB (BER = 4.16×10^{-2}) to 4.86 dB (BER = 4.01×10^{-2}), which correspond to the typical Q (BER) threshold of the state-of-the-art SD-FEC having a code rate of 0.8 [31], [32]. Considering this fact, we will use 0.85 as a target of the normalized GMI throughout the paper.

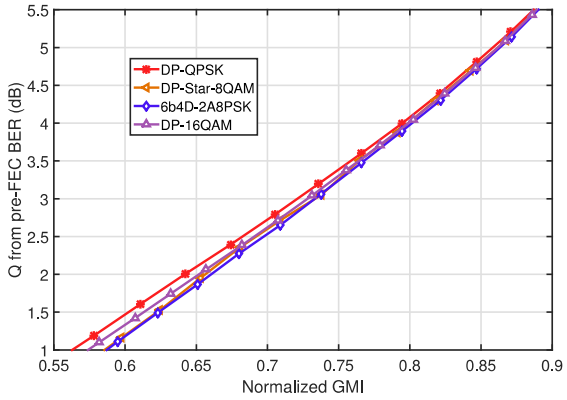

Fig. 1. Q-factor calculated from pre-FEC BER vs. normalized GMI for four modulation formats.

B. Generic 2A8PSK

The constellation of the 4D-2A8PSK family [21]–[24] is shown in Fig. 2. It is essentially 8PSK, with two different amplitudes represented by the radii, r_1 and r_2 (suppose $r_1 \le r_2$ without loss of generality). For the combined X- and Y-polarizations (i.e., 4D space), there are $2^8 = 256$ possible combinations (i.e., 8 bits per 4D symbol). By superimposing a condition that two polarizations have complimentary radius, i.e., if r_1 is chosen for one polarization, then r_2 is used for the other polarization, we can realize set partitioned (SP) 4D codes, achieving 4D constant modulus property, leading to excellent nonlinear transmission characteristics. We define r_1/r_2 $(\leqslant 1)$ as a ring ratio. If the ring ratio is equal to 1, the modulation format is reduced to regular DP-8PSK.

Fig. 2 also includes the mapping rule of 4D-2A8PSK [33]. Set-partitioning can be applicable. Letting $B[0],\ldots,B[7]$ denote eight bits for modulation, $B[0]$–$B[2]$ and $B[3]$–$B[5]$ are used for the Gray-mapped 8PSK at X- and Y-polarizations, respectively. Whereas, $B[6]$ and $B[7]$ are used to determine the amplitude in X- and Y-polarizations, respectively. By properly choosing the best 32, 64, and 128 point constellations out of 256 combinations, we can obtain 32SP-, 64SP-, and 128SP-2A8PSK, for the spectral efficiency of 5, 6, and 7 bits/symbol, respectively. We also call them 5b4D-, 6b4D-, and 7b4D-2A8PSK for convenience.

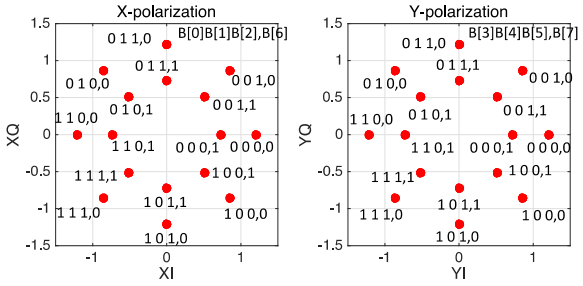

Fig. 2. Constellation and bit-to-symbol mapping of 2A8PSK.

C. 5b4D-2A8PSK

For 5 bits/symbol, 5b4D-2A8PSK (i.e., 32SP-2A8PSK) can be constructed by a linear code, with five information (modulation) bits $B[0]$–$B[4]$, and three parity bits $B[5]$–$B[7]$. Since $B[5]$ and $B[6]$ each can be expressed as the linear combination of the five information bits, the total number of possible linear codes to be designed is $2^{10} = 1024$. We selected the best combination which gives the least required SNR for the target GMI of 0.85, through Monte-Carlo simulations.

In order to realize a 4D constant modulus format, the Y-polarization ring size is always the opposite of the X-polarization ring size. This is expressed by negating another parity bit $B[6]$ for $B[7]$. Consequently, the parity-check equations for 5b4D-2A8PSK are expressed as follows:

$$B[5] = B[0]\oplus B[1]\oplus B[2], \quad (3)$$

$$B[6] = B[2]\oplus B[3]\oplus B[4], \quad (4)$$

$$B[7] = \overline{B[6]}, \quad (5)$$

where $\oplus$ and $\overline{[\cdot]}$ denote the modulo-2 addition and negation, respectively. This code shows 0.25 dB improvement in the

required SNR in the linear region compared to that of [24], which was constructed as a nonlinear code.

D. 6b4D-2A8PSK

In the case of 6b4D-2A8PSK (64SP-2A8PSK), $B[6]$ is a parity bit of single-parity-check code which is an exclusive-or (XOR) of all the information bits $B[0]$–$B[5]$, protecting all information bits. Another parity bit $B[7]$ is the negation of $B[6]$ as used in 7b4D-2A8PSK. The best code for the target GMI of 0.85 (which we call Type A) was found to be

$$B[6] = B[0] \oplus B[1] \oplus B[2] \oplus B[3] \oplus B[4] \oplus B[5], \quad (6)$$

$$B[7] = \overline{B[6]}. \quad (7)$$

Note that this is the same code as described in [21]. For comparison, we also consider another code (which we call Type B), which uses a parity bit $B[6]$ to protect only the least significant bits, as follows:

$$B[6] = B[2] \oplus B[5], \quad (8)$$

$$B[7] = \overline{B[6]}. \quad (9)$$

The normalized GMI for these two types, after optimizing the ring ratio at each SNR, is plotted in Fig. 3. The optimized ring ratio is also present. As the figure shows, in the region where the GMI is below 0.81, Type B slightly outperforms Type A. On the other hand, for GMI above 0.81, Type A performs better than Type B. Since our target GMI is 0.85, we use Type A for 6b4D-2A8PSK throughout this paper.

Note that, for Type A, the optimal ring ratio becomes 1 when SNR is below 6 dB. This means that a simple DP-8PSK performs almost as well as Type B. It is related to the report in [34], where low-rate (at a target GMI of 0.567) DP-8PSK was shown to perform better than high-rate (at a target GMI of 0.85) DP-QPSK.

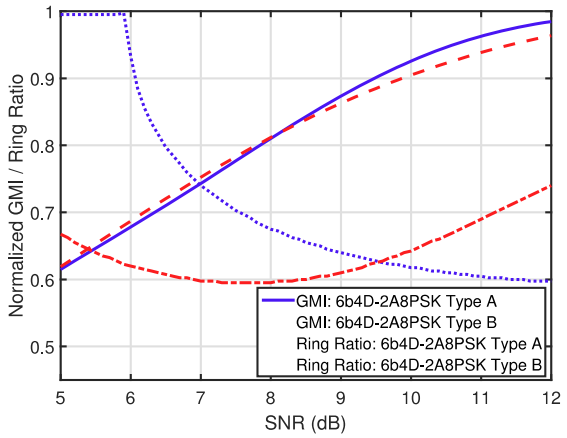

Fig. 3. Normalized GMI and optimized ring ratio vs. SNR in AWGN for the two types of 6b4D-2A8PSK.

E. 7b4D-2A8PSK

The simplest code in the 4D constant modulus 2A8PSK family is 7b4D-2A8PSK, which can also be considered as 128SP-2A8PSK. In this case, $B[0]$–$B[6]$ are the information bits while there is only one parity bit at $B[7]$. In order to realize 4D constant modulus format, a single parity bit $B[7]$ is used as follows:

$$B[7] = \overline{B[6]}. \quad (10)$$

F. Other Modulation Formats

In order to evaluate the performance of 5b4D-2A8PSK, we consider three other modulation formats having 5 bits/symbol spectral efficiency; i.e., 8PolSK-QPSK [35], 32SP-16QAM [8], and time-domain hybrid (TDH) modulation. 8PolSK-QPSK [35] is a 4D constant modulus format, which has 8 polarization states on the Poincaré sphere. 32SP-16QAM is a 4D modulation which is based on DP-16QAM. We used the parity rule described in [8] to generate 32 code words. We also evaluated TDH modulation using a 1:1 mixture of DP-QPSK and 6b4D-2A8PSK to generate 5 bits/symbol spectral efficiency on average.

For comparison with 6b4D-2A8PSK, we evaluated three other modulation formats of 6 bits/symbol spectral efficiency; specifically, DP-8PSK, DP-Star-8QAM, and DP-Circular-8QAM [18]. DP-8PSK and DP-Star-8QAM are standard modulation formats. DP-Circular-8QAM has one center point and seven circular constellation points, and has larger Euclidean distance than DP-8PSK. We followed the constellation and labeling as described in [18].

For 7b4D-2A8PSK comparison, two more modulation formats of 7 bits/symbol spectral efficiency are evaluated. 128SP-16QAM is a 4D modulation based on DP-16QAM, where the parity rule described in [8] is used to generate 128 code words. TDH modulation using 1:1 mixture of 6b4D-2A8PSK and DP-16QAM is also simulated. In addition, we simulated $(7/8)\times$34GBd DP-16QAM to compare for the same data rate.

III. Nonlinear Transmission Characteristics

A. Simulation Procedure

We simulated transmission performance over a 2,000 km DM link at a rate of 34 GBaud per channel to investigate the effect of high fiber nonlinearity. Simulation procedures are similar to that reported in the previous work [24]. Fig. 4 depicts the configuration and the computational procedure for nonlinear transmission simulations.

At the transmitter, pulses were filtered by a root-raised-cosine (RRC) filter with a roll-off factor of 10%. Eleven WDM channels using the same modulation format were simulated with 37.5 GHz spacing and no optical filtering. The link comprised 25 spans of 80 km non-zero dispersion shifted fiber (NZDSF) with loss compensated by Erbium-doped fiber amplifiers (EDFAs). In order to quantify performance over the nonlinear fiber link for multiple modulation formats, a span loss budget was used as a performance metric [36], which is defined as,

$$\begin{aligned}\text{Span Loss Budget} = 58 + P - \text{ROSNR} \\ - 10\log_{10}(N) - \text{NF}, \end{aligned} \quad (11)$$

where P is the launch power per channel expressed in dBm, ROSNR is the required OSNR to achieve the target GMI in

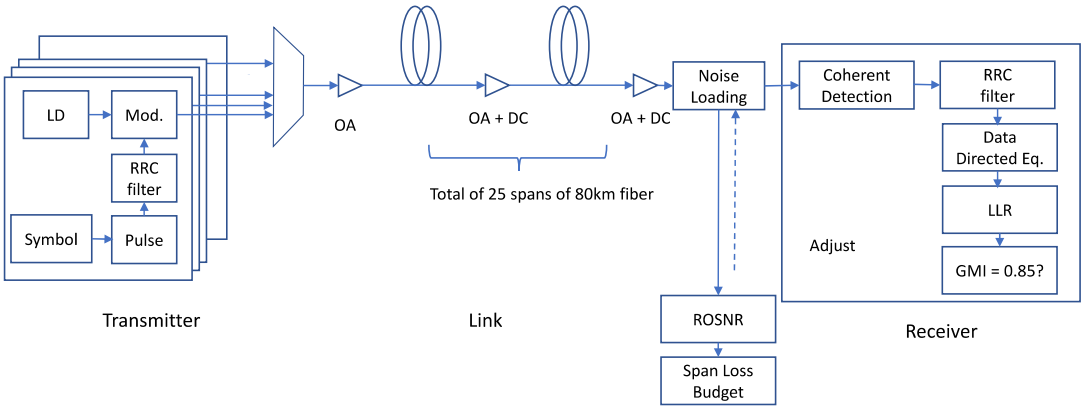

Fig. 4. Configuration of the simulated system and the procedure. LD: Laser Diode, RRC: Root Raised Cosine, OA: Optical Amplifier, DC: Dispersion Compensation, LLR: Log-Likelihood Ratio, ROSNR: Required OSNR.

dB, N is the number of spans, and NF is the noise figure of the EDFAs in dB.

NZDSF parameters were, $\gamma = 1.6$ /W/km; $D = 3.9$ ps/nm/km; $\alpha = 0.2$ dB/km. Other fiber effects such as dispersion slope and polarization mode dispersion (PMD) were not simulated. At the end of each span, 90% of the chromatic dispersion was compensated as a lumped linear dispersion compensator. Dispersion pre-compensation was applied at the transmitter side using 50% of the residual dispersion of the full link. The rest of the dispersion is compensated just before the receiver.

An ideal homodyne coherent receiver was used, with an RRC filter with a roll-off factor of 10%, followed by sampling at twice the symbol rate. For adaptive equalization, we used a time-domain data-aided least-mean-square equalizer which uses the transmitted data directly as the training sequences for simplicity. A discussion on a more realistic equalizer will be given in Section V. We did not use carrier phase estimation (CPE) in Sections III and IV.

All the optical noise due to the EDFA is loaded just before the receiver. In order to evaluate the system margin, we varied the optical signal-to-noise ratio (OSNR) with excessive noise loading such that the target GMI is reached. The obtained required OSNR is used to calculate the span loss budget as in (11). An EDFA noise figure of 5 dB is assumed for the span loss budget calculations.

Note that in DM links it is known that there is some difference in simulated nonlinear transmission performance between having all noise loaded at the receiver (our case) and distributed noise at each EDFA, depending on the modulation format [37]. For XPolM and WDM (SPM+XPM+XPolM) cases the difference is generally small, whilst for SPM and XPM the noise-loaded case may somewhat underestimate the nonlinear impact (where the performance gap is smaller at baud rates ≥ 28 GBaud). More detailed analysis regarding this gap is beyond the scope of this work.

B. 5 bits/symbol Formats

Four 5 bit/symbol formats were compared as shown in Fig. 5. In this case, the ring ratio $r_1/r_2 = 0.61$ is optimized for

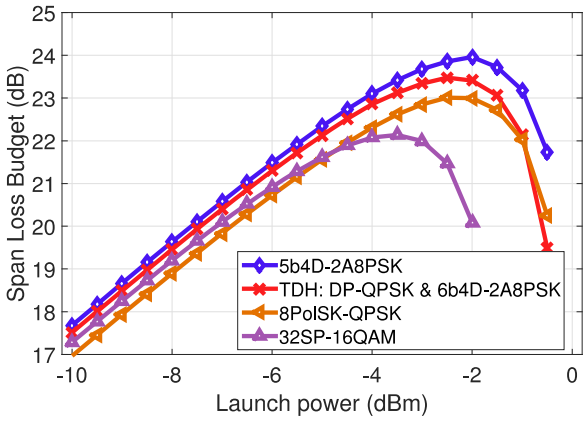

Fig. 5. Span loss budget of four 5 bits/symbol modulation formats as a function of launch power for the DM link.

5b4D-2A8PSK for maximizing the span loss budget. Note that ring ratio is not a sensitive parameter, and in fact between 0.56 and 0.66, the peak span loss budget changed only by 0.03 dB.

The span loss budget for 32SP-16QAM reduces quickly due to large power variations, since it is based on 16QAM. On the other hand, 8PolSK-QPSK [35] has 0.65 dB worse OSNR for the linear case, the saturation characteristics is very similar to 5b4D-2A8PSK, due to its 4D constant modulus property. TDH modulation using a 1:1 mixture of DP-QPSK and 6b4D-2A8PSK has constant modulus property at each time slot. However, we used an optimized power allocation for TDH modulation (i.e., 6b4D-2A8PSK has 2.7 dB higher power than DP-QPSK), and there is a power fluctuation between time slots, causing some penalty due to the nonlinearity.

Overall, 5b4D-2A8PSK has the higher maximum span loss budget by 0.5 dB over the TDH modulation, by 0.9 dB over 8PolSK-QPSK, and by 1.8 dB over 32SP-16QAM.

C. 6 bits/symbol Formats

Four 6 bits/symbol modulation formats were compared as in Fig. 6. The optimized ring ratio was $r_1/r_2 = 0.65$ for 6b4D-2A8PSK to maximize the span loss budget. It is observed that

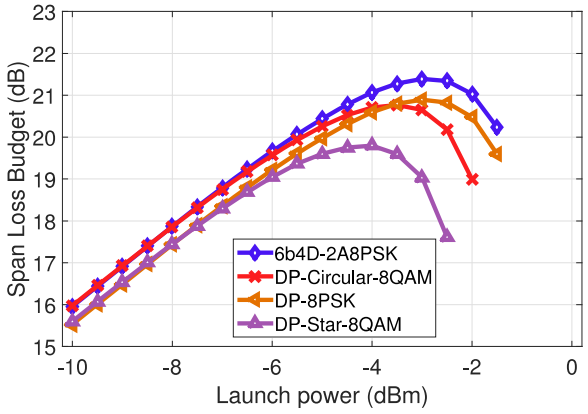

Fig. 6. Span loss budget of four 6 bits/symbol modulation formats for the DM link.

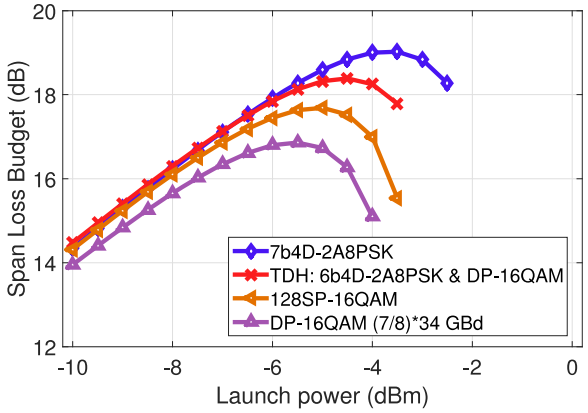

Fig. 7. Span loss budget of three 7 bits/symbol modulation formats at 34 GBd and DP-16QAM with the same data rate ($7/8 \times 34$ GBd) as a function of launch power for the DM link.

the maximum span loss budget for 6b4D-2A8PSK is higher than DP-Circular-8QAM, DP-8PSK, and DP-Star-8QAM by 0.6 dB, 0.5 dB, and 1.6 dB, respectively.

D. 7 bits/symbol Formats

Fig. 7 shows performance comparison among three 7 bit/symbol formats at 34 GBd and DP-16QAM of the same data rate ($7/8 \times 34$ GBd). Here, the ring ratio of $r_1/r_2 = 0.59$ is chosen for 7b4D-2A8PSK to maximize the span loss budget. Here, TDH modulation uses a 1:1 mixture of 6b4D-2A8PSK and 128SP-QAM, whose optimized power ratio was 0.1 dB.

We can see that 7b4D-2A8PSK outperformed THD modulation, 128SP-16QAM, and $(7/8) \times 34$GBd DP-16QAM by 0.7 dB, 1.4 dB, and 2.2 dB, respectively.

E. Summary for DM Link

The summary of the peak span loss budget for the DM link is shown in Fig. 8. The circles connected by the dashed lines include DP-QPSK, 5b4D-, 6b4D-, 7b4D-2A8PSK, and DP-16QAM, all at 34 GBd. Squares are taken from TDH modulation formats, and triangles are from other modulation formats

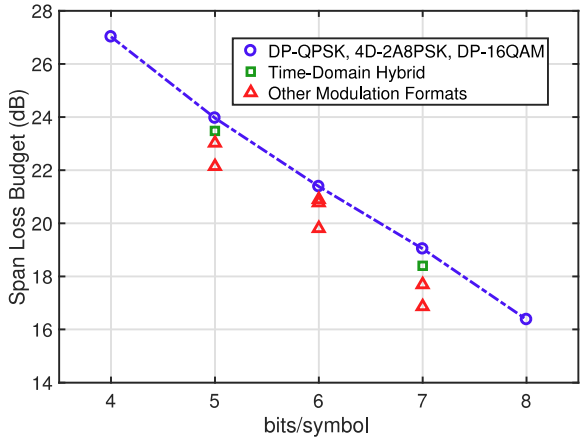

Fig. 8. Summary of the peak span loss budget for the DM link. Blue circles connected with lines are for the three 4D-2A8PSK formats, DP-QPSK, and DP-16QAM. Green squares are for TDH modulation formats, and red triangles are for other modulation formats shown in Figs. 5–7.

in Figs. 5–7. This shows that the 4D-2A8PSK family fills the gap between DP-QPSK and DP-16QAM almost linearly (in the dB domain), and each one offers a solid improvement compared to the conventional modulation formats. Also, note that DP-QPSK is a member of 4D-2A8PSK family with specific parity-check equations and ring ratio of 1.

F. 5 bits/symbol in Dispersion Uncompensated Link

In order to evaluate the transmission characteristics of various modulation formats under a reduced nonlinearity situation, we also simulated the link with 50 spans of 80 km standard single mode fiber (SSMF) without inline dispersion compensation. SSMF parameters are, $\gamma = 1.2$ /W/km; $D = 17$ ps/nm/km; $\alpha = 0.2$ dB/km. No dispersion pre-compensation was used. The target GMI remained the same at 0.85. Fig. 9 shows the span loss budget of the four modulation formats for the spectral efficiency of 5 bits/symbol, as an example. Overall, the differences among the modulation formats are smaller than the case of DM-NZDSF link. 5b4D-2A8PSK still shows the highest budget, outperforming TDH of DP-QPSK and 6b4D-2A8PSK, 8PolSK, and 32SP-8QAM by 0.2 dB, 1.0 dB, and 0.8 dB, respectively. For dispersion uncompensated links, TDH and 32SP-16QAM did not suffer as much as they did in the DM case. This may be due to the weaker nonlinear distortion in the uncompensated SSMF links compared to DM-NZDSF links.

G. Remarks

Here, we make some remarks in the differences between the preliminary results reported in [24] and the new results shown in Figs. 5 and 7 of this paper. Both simulation procedures are identical, except for two factors. In this paper, we used an improved step-size factor μ for the least-mean-square equalizer and also corrected the transmitter pulse shape. For the second factor, more specifically, in [24], we have included an additional sample-hold function followed by an RRC filter for the pulse shape, while in this paper we used a delta function

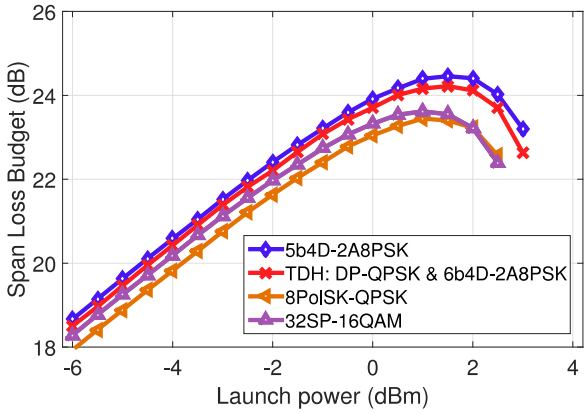

Fig. 9. Span loss budget of four 5 bits/symbol modulation formats as a function of launch power for the dispersion unmanaged link.

followed by an RRC filter to meet the Nyquist condition. These modified factors led to approximately 0.35 dB and 0.5 dB improvements in the span loss budget in the linear region and at the peak, respectively, regardless of the modulation formats. In addition, we modified the following three modulation formats. 1) 5b4D-2A8PSK is improved by using different parity-check equations as described in Section II-C. 2) We previously used a sub-optimal code for 32SP-16QAM. We now use an optimized code described in [8]. 3) For 7 bits/symbol TDH modulation of 6b4D-2A8PSK and DP-16QAM, we refined the power ratio to achieve the highest budget.

IV. Separated Nonlinear Effects

In order to understand the source of the benefit of 4D constant modulus modulation, we conducted additional simulations with separated nonlinear components, based on the method proposed in [38]. Using this method, we can evaluate the nonlinear transmission performance with selective nonlinear effects of SPM, XPM, and XPolM.

In Fig. 10, we plot the calculated Q-factor as a function of the OSNR for 6b4D-2A8PSK and DP-Star-8QAM in the DM link (same simulation parameters as Section III-A). Here, we use the recently proposed Q-factor definition based on GMI not pre-FEC BER, as follows [33]:

$$Q^2_{\mathrm{GMI}} = \{0.5 \cdot J^{-1}(\mathrm{GMI})\}^2, \tag{12}$$

where $J^{-1}(\cdot)$ is the inverse J function, widely used in extrinsic information transfer chart analysis [28]. The inverse J function is well approximated by

$$J^{-1}(I) \simeq \begin{cases} a_1 I^2 + b_1 I + c_1\sqrt{I}, & 0 \le I \le I^*, \\ -a_2 \ln[b_2(1-I)] - c_2 I, & I^* \le I \le 1, \end{cases} \tag{13}$$

$$\begin{aligned} &I^* = 0.3646, \\ &a_1 = 1.09542, \quad b_1 = 0.214217, \quad c_1 = 2.33727, \\ &a_2 = 0.706692, \quad b_2 = 0.386013, \quad c_2 = -1.75017. \end{aligned}$$

The above Q-factor based on GMI in (12) is a generalized extension from the conventional Q-factor based on BER in (2) so

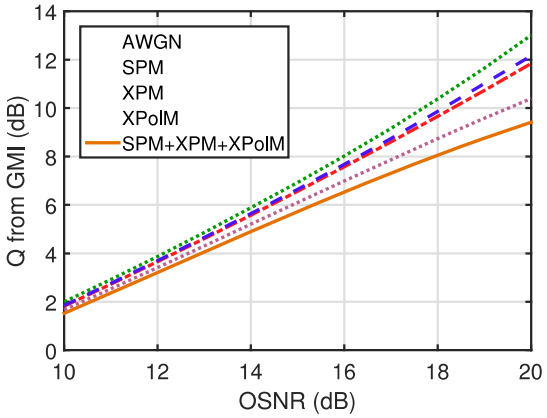

(a) 6b4D-2A8PSK

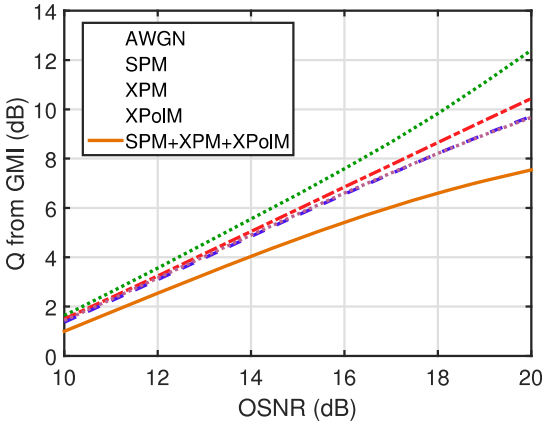

(b) DP-Star-8QAM (Curves for XPM and XPolM overlapping)

Fig. 10. Q-factor as a function of OSNR for 6b4D-2A8PSK and DP-Star-8QAM with separated nonlinear effects at a launch power of -4 dBm.

that we can measure the effective SNR to achieve same post-FEC BER performance with SD-FEC systems. While both definitions provide exactly same Q performance in binary-input AWGN channels, the generalized Q-factor can predict SNR gain more accurately compared to the conventional Q-factor for BICM systems using high-order high-dimensional modulation and SD-FEC coding.

The curves denoted with 'AWGN' in Fig. 10 show the case when the nonlinear effects are ignored, and the curves represented with 'SPM', 'XPM', and 'XPolM' indicate that these nonlinear components are added individually. The curve with 'SPM+XPM+XPolM' shows the case when all of these nonlinear effects are taken into account. The launch power is set to be -4 dBm, which gives the maximum span loss budget for DP-Star-8QAM. OSNR of 15.2 dB corresponds to a normalized GMI of 0.85 at this launch power.

Fig. 11 re-plots the simulated Q versus separated nonlinearity under the condition of 15.2 dB OSNR. Q in the linear case (AWGN) is higher for 6b4D-2A8PSK than DP-Star-8QAM by 0.4 dB. The contributions from SPM and XPM in 6b4D-2A8PSK are much smaller than those in DP-Star-8QAM. It verifies that 4D-2A8PSK family can be robust against XPM and SPM nonlinearity. On the other hand, the contribution

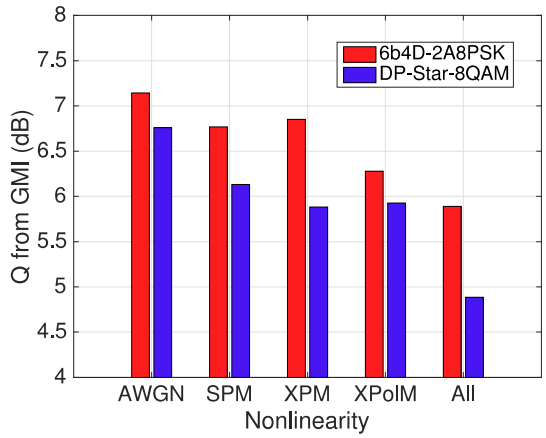

Fig. 11. Q-factor for 6b4D-2A8PSK and DP-Star-8QAM with separated nonlinear effects at a launch power of -4 dBm and OSNR of 15.2 dBm.

of XPolM is similar in 6b4D-2A8PSK and DP-Star-8QAM (more specifically, Q degradation from AWGN is comparable for both modulation formats). This is because power in the individual polarization in 6b4D-2A8PSK fluctuates over symbol time even though this has a 4D constant modulus property. This result is consistent with the report in [35], where another 4D constant modulus modulation format 8PolSK shows a significant reduction in SPM and XPM, but not XPolM.

As explained in Section III-A, we assumed PMD to be zero. In reality, PMD varies from fiber plant to fiber plant, and XPolM is generally decreased by higher PMD [39]. As shown in Figs. 10–11, the dominant nonlinear degradation for 4D-2A8PSK comes from XPolM, and hence, the benefit of 4D-2A8PSK family may be even more significant in the presence of high PMD.

V. DSP Algorithm

So far, in order to analyze the fundamental potential of 4D-2A8PSK family, we used an idealized data-directed least-mean-square equalizer. In this section, we briefly address the performance impact with more realistic equalizers [40], [41] for practical implementation.

First, we consider a conventional radius-directed equalizer (RDE) [41] for 6b4D-2A8PSK, where the decision on the ring is carried out on each polarization independently. In this case, we observed a degradation of 0.12 dB and 0.10 dB in span loss budget compared to the idealized least-mean-square equalizer, respectively, at a launch power of -10 dBm and -4 dBm.

We then took advantage of 4D constant modulus property, by using the relative power of polarizations for soft decision of the ring radii. For soft-decision information, we used a sigmoid function $S(x) = 1/(1 + e^{-x/a})$, where a is a parameter to determine the softness, and x is a relative power of two polarizations. In this manner, we could compensate for the degradation by 0.07 dB from the conventional RDE. Overall, the net degradation due to the realistic adaptive equalizer compared to the ideal one is no greater than 0.05 dB.

VI. Conclusion

We reviewed the recently proposed 5, 6, and 7 bits/symbol 4D modulation format family based on 2A8PSK. A series of nonlinear transmission simulation results revealed that this modulation format family outperforms the conventional modulation formats at each corresponding spectral efficiency, in particular for highly nonlinear DM links. It was also confirmed that the primary benefit of the 4D constant modulus property comes from the reduction of SPM and XPM. In addition, we showed that the realistic adaptive equalizer will result in no more than 0.05 dB penalty when the constant modulus property is exploited for the radius decision. Since these modulation formats differ just in the parity bits, they can be realized with very similar hardware over different spectral efficiency between DP-QPSK and DP-16QAM.

References

[1] M. Jinno, B. Kozicki, H. Takara, A. Watanabe, Y. Sone, T. Tanaka, and A. Hirano, "Distance-adaptive spectrum resource allocation in spectrum-sliced elastic optical path network," *IEEE Commun. Mag.*, vol. 48, no. 8, pp. 138–145, 2010.

[2] A. Nag, M. Tornatore, and B. Mukherjee, "Optical network design with mixed line rates and multiple modulation formats," *J. Lightw. Technol.*, vol.28, no. 4, pp. 466–475, 2010.

[3] A. Alvarado, D. J. Ives, S. J. Savory, and P. Bayvel, "On the impact of optimal modulation and FEC overhead on future optical networks," *J. Lightw. Technol.*, vol. 34,, no. 9, pp. 2339–2352, 2016.

[4] D. J. Ives, A. Alvarado, and S. J. Savory, "Adaptive transceivers in nonlinear flexible networks," in *European Confrence on Optical Communication*, 2016, Düsseldorf, Germany, Paper M.1.B.1.

[5] E. Agrell and M. Karlsson, "Power-efficient modulation formats in coherent transmission systems," *J. Lightw. Technol.*, vol. 27, no. 22, pp. 5115–5126, 2009.

[6] R.-J. Essiambre, G. Kramer, P. J. Winzer, G. J. Foschini, and B. Goebel, "Capacity Limits of Optical Fiber Networks," *J. Lightw. Technol.*, vo. 28, no. 4, pp. 662–701, 2010.

[7] G. Bosco, V. Curri, A. Carena, P. Poggiolini, and F. Forghieri, "On the performance of Nyquist-WDM terabit superchannels based on PM-BPSK, PM-QPSK, PM-8QAM or PM-16QAM subcarriers," *J. Lightw. Technol.*, vo. 29, no. 1, pp. 53–61, 2011.

[8] J. Renaudier, A. Voicila, O. Bertran-Pardo, O. Rival, M. Karlsson, G. Charlet, and S. Bigo, "Comparison of set-partitioned two-polarization 16QAM formats with PDM-QPSK and PDM-8QAM for optical transmission systems with error-correction coding," in *European Conf. Optical Communications*, 2012, Amsterdam, The Netherlands, Paper We.1.C.5.

[9] Q. Zhuge, X. Xu, M. Morsy-Osman, M. Chagnon, M. Qiu, and D. V. Plant, "Time domain hybrid QAM based rate-adaptive optical transmissions using high speed DACs," in *Optical Fiber Commun. Conf.*, 2013, Anaheim, CA, Paper OTh4E.6.

[10] J. K. Fischer, S. Alreesh, R. Elschner, F. Frey, M. Nölle, C. Schubert, "Bandwidth-variable transceivers based on 4D modulation formats for future flexible networks," in *European Conf. Optical Communications*, 2013, London, UK, Paper Tu.3.C.1.

[11] D. S. Millar, T. Koike-Akino, S. Ö. Arik, K. Kojima, T. Yoshida, and K. Parsons, "High-dimensional modulation for coherent optical communications systems," *Opt. Exp.*, vol. 22, no. 7, pp. 8798–8812, 2014.

[12] D. S. Millar, T. Koike-Akino, S. Ö. Arik, K. Kojima, and K. Parsons, "Comparison of quaternary block-coding and sphere-cutting for high-dimensional modulation," in *Optical Fiber Commun. Conf.*, 2014, San Francisco, CA, Paper M3A.4.

[13] M. Reimer, S. O. Gharan, A. D. Shiner, and M. O'Sullivan, "Optimized 4 and 8 dimensional modulation formats for variable capacity in optical networks," in *Optical Fiber Commun. Conf.*, 2016, Anaheim, CA, Paper M3A.4.

[14] T. Koike-Akino, K. Kojima, D. S. Millar, K. Parsons, T. Yoshida, and T. Sugihara, "Pareto-efficient set of modulation and coding based on RGMI in nonlinear fiber transmissions," in *Optical Fiber Commun. Conf.*, 2016, Anaheim, CA, Paper Th1D.4.

[15] T. Koike-Akino, K. Kojima, D. S. Millar, K. Parsons, T. Yoshida, and T. Sugihara, "Pareto optimization of adaptive modulation and coding set in nonlinear fiber-optic systems," *J. Lightw. Technol.*, vol. 35, no. 3, pp.1-9, 2017.

[16] M. Sjödin, E. Agrell, and M. Karlsson, "Subset-optimized polarization-multiplexed PSK for fiber-optic communications," *IEEE Comm. Lett.*, vol. 17, no. 5, pp. 838–840, 2013.

[17] H. Buelow, X. Lu, L. Schmalen, A. Klekamp, and F. Buchali, "Experimental performance of 4D optimized constellation alternatives for PM-8QAM and PM-16QAM," in *Optical Fiber Commun. Conf.*, 2014, San Francisco, CA, Paper M2A.6.

[18] R. Rios-Mueller, J. Renaudier, L. Schmalen, and G. Charlet, "Joint coding rate and modulation format optimization for 8QAM constellations using BICM mutual information," in *Optical Fiber Commun. Conf.*, 2015, Los Angeles, CA, Paper W3K.4.

[19] S. Zhang, K. Nakamura, F. Yaman, E. Mateo, T. Inoue, Y. Inada, "Optimized BICM-8QAM formats based on generalized mutual information," in *European Conf. Optical Communications*, 2015, Valencia, Spain, Paper Mo.3.6.5.

[20] T. Nakamura, E. L. T. d. Gabory, H. Noguchi, W. Maeda, J. Abe, and K. Fukuchi, "Long haul transmission of four-dimensional 64SP-12QAM signal based on 16QAM constellation for longer distance at same spectral efficiency as PM-8QAM," in *European Conf. Optical Communications*, 2015, Valencia, Spain, Paper Th.2.2.2.

[21] K. Kojima, D. S. Millar, T. Koike-Akino, and K. Parsons, "Constant modulus 4D optimized constellation alternative for DP-8QAM," in *European Conf. Optical Communications*, 2014, Cannes, France, Paper P.3.25.

[22] K. Kojima, T. Koike-Akino, D. S. Millar, and K. Parsons, "BICM capacity analysis of 8QAM-alternative modulation formats in nonlinear fiber transmission," *Tyrrhenian Int'l Workshop on Digital Comm.*, 2015, Florence, Italy, Paper P.4.5.

[23] K. Kojima, T. Koike-Akino, D. S. Millar, T. Yoshida, and K. Parsons, "BICM capacity analysis of 8QAM-alternative 2D/4D modulation formats in nonlinear fiber transmission," in *Conf. Lasers and Electro-Optics*, 2016, Anaheim, Paper SM2F.5.

[24] K. Kojima, T. Yoshida, T. Koike-Akino, D. S. Millar, K. Parsons, and V. Arlunno, "5 and 7 bit/symbol 4D Modulation Formats Based on 2A8PSK," in *European Conf. Optical Communications*, 2016, Düsseldorf, Germany, Paper W.2.D.1.

[25] A. Alvarado, E. Agrell, D. Lavery, and P. Bayvel, "LDPC codes for optical channels: Is the "FEC Limit" a good predictor of post-FEC BER?" in *Optical Fiber Commun. Conf.*, 2015, Los Angeles, CA, Paper Th3E.5.

[26] A. Alvarado and E. Agrell, "Four-dimensional coded modulation with bit-wise decoders for future optical communications," *J. Lightw. Technol.*, vol. 33, no. 10, pp. 1993–2003, 2015.

[27] R. Maher, A. Alvarado, D. Lavery, and E. P. Bayvel, "Modulation order and code rate optimisation for digital coherent transceivers using generalised mutual information," in *European Conf. Optical Communications*, 2015, Valencia, Spain, Paper M.3.3.4.

[28] S. ten Brink, G. Kramer, and A. Ashikhmin, "Design of low-density parity-check codes for modulation and detection," *IEEE Trans. Commun.*, vol. 52, no. 4, pp. 670–678, Apr. 2004.

[29] A. Bennatan and D. Bushtein, "Design and analysis of nonbinary LDPC codes for arbitrary discrete-memoryless channels," *IEEE Trans. Inf. Theory*, vol. 52, no. 2, pp. 549–583, 2006.

[30] L. Szczecinski and A. Alvarado, *Bit-interleaved coded modulation: Fundamentals, analysis, and design*, Wiley, UK, 2015, p. 228.

[31] S. Zhang, M. Arabaci, F. Yaman, I. B. Djordjevic, L. Xu, T. Wnag, Y. Inada, T. Ogata, and Y. Aoki, "Experimental study of non-binary LDPC coding for long-haul coherent optical QPSK transmissions," *Opt. Exp.*, vol. 19, no. 20, pp. 19042–19049, 2011.

[32] K. Sugihara, Y. Miyata, T. Sugihara, K. Kubo, H. Yoshida, W. Matsumoto, and T. Mizuochi, "A spatially-coupled type LDPC code with an NCG of 12 dB for optical transmission beyond 100 Gb/s," in *Optical Fiber Commun. Conf.*, 2013, Anaheim, CA, Paper OM2B.4.

[33] T. Yoshida, K. Matsuda, K. Kojima, H. Miura, D. Dohi, M. Pajovic, T. Koike-Akino, D. S. Millar, K. Parsons, and T. Sugihara, "Hardware-efficient precise and flexible soft-demapping for multi-dimensional complementary APSK signals," in *European Conf. Optical Communications*, 2016, Düsseldorf, Germany, Paper Th.2.P2.SC3.27.

[34] K. Kojima, T. Koike-Akino, D. S. Millar, M. Pajovic, K. Parsons, and T. Yoshida,, "Investigation of low code rate DP-8PSK as an alternative to DP-QPSK," in *Optical Fiber Commun. Conf.*, 2016, Anaheim, CA, Paper Th1D.2.

[35] M. Chagnon, M. Osman, Q. Zhuge, X. Xu, and D. V. Plant, "Analysis and experimental demonstration of novel 8PolSK-QPSK modulatoin at 5 bis/symbol for passive mitigation of nonlinear impairments," *Opt. Exp.*, vol. 21, no. 25, pp. 30204–30220, 2013.

[36] P. Poggiolini, G. Bosco, A. Carena, V. Curri, and F. Forghieri, "Performance evaluation of coherent WDM PS-QPSK (HEXA) accounting for non-linear fiber propagation effects," *Opt. Exp.*, vol. 18, no. 11, pp. 11360–11371, 2010.

[37] N. Rossi, P. Serena, and A. Bononi, "Symbol-rate dependence of dominant nonlinearityand reach in coherent WDM links," *J. Lightw. Technol.*, vol. 33, no. 14, pp. 3132–3143, 2009.

[38] A. Bononi, P. Serena, N. Rossi, and D. Sperti, "Which is the dominant nonlinearity in long-haul PDM-QPSK coherent transmissions?," in *European Conf. Optical Communications*, 2010, Torino, Italy, Paper Th.10.E.1.

[39] M. Winter, C.-A. Burge, D. Setti, and K. Petermann, "A statistical treatment of cross-polarization modulation in DWDM systems," *J. Lightw. Technol.*, vol. 27, no. 17, pp. 3739–3751, 2009.

[40] M. Pajovic, D. S. Millar, T. Koike-Akino, R. Maher, D. Lavery, A. Alvarado, M. Paskov, K. Kojima, K. Parsons, B. C. Thomsen, S. J. Savory, and P. Bayvel, "Experimental demonstration of multi-pilot aided carrier phase estimation for DP-16QAM and DP-256QAM," in *European Conf. Optical Communications*, 2015, Valencia, Spain, Paper Mo.4.3.3.

[41] M. J. Ready and R. P. Gooch, "Blind equalization based on radius directed adaptation," *Proc. of ICASSP*, vol. 3, pp. 1699–1702, 1990.

Keisuke Kojima (S'82–M'84–SM'13) was born in Hokkaido, Japan, in 1958. He received the B.S., M.S., and Ph.D. degrees in electrical engineering from the University of Tokyo, Tokyo, Japan, in 1981, 1983, and 1990, respectively. He also received the M.S. degree from the University of California, Berkeley, CA, USA, in 1982. He worked for eight years at the Central Research Laboratory, Mitsubishi Electric Corp., from 1983 on the research of narrow linewidth lasers and DFB and DBR lasers. He spent nine years at AT&T/Lucent Bell Laboratories on the R&D of uncooled Fabry–Perot and DFB lasers, vertical-cavity surface-emitting lasers, passive optical network systems, and metro optical systems, first as a Member of Technical Staff, and later as a Technical Manager. He also worked at Agere Systems, Denselight Semiconductors, and TriQuint Semiconductors on optical devices and modules, and optical systems testbed. He has been with Mitsubishi Electric Research Laboratories, Cambridge, MA, USA, since 2005, where he is currently working on the R&D of photonic-integrated circuits and coherent optical systems, as a Senior Principal Research Scientist. He has more than 170 publications in journals and conference proceedings. He is a Fellow of the Optical Society of America.

Tsuyoshi Yoshida (M'09) received the B.S. degree in electrical and electronic engineering and and M.S. degree in communications and computer engineering from Kyoto University, Kyoto, Japan, in 2005 and 2007, respectively. Since 2007, he has been with Mitsubishi Electric Corporation, Kamakura, Japan, where he has been engaged in research and development of high-speed optical transceiver, coding and modulation, fiber nonlinearity mitigation, practical digital signal processing being suitable to hardware implementation for efficient optical transmissions. He is currently also with Department of Microtechnology and Nanoscience, Chalmers University of Technology.

Toshiaki Koike-Akino (M'05–SM'11) received the B.S. degree in electrical and electronics engineering, M.S. and Ph.D. degrees in communications and computer engineering from Kyoto University, Kyoto, Japan, in 2002, 2003, and 2005, respectively. During 2006–2010 he was a Postdoctoral Researcher at Harvard University, and joined Mitsubishi Electric Research Laboratories, Cambridge, MA, USA, in 2010. His research interests include digital signal processing for data communications and sensing. He received the YRP Encouragement Award 2005, the 21st TELECOM System Technology Award, the 2008 Ericsson Young Scientist Award, the IEEE GLOBECOM'08 Best Paper Award in Wireless Communications Symposium, the 24th TELECOM System Technology Encouragement Award, and the IEEE GLOBECOM'09 Best Paper Award in Wireless Communications Symposium.

David S. Millar (S'07–M'11) was born in Manchester, U.K., in 1982. He received the M.Eng. degree in electronic and communications engineering from the University of Nottingham, Nottingham, U.K. in 2007, and the Ph.D. degree in optical communications from University College London, London, U.K., in 2011. He is currently working at Mitsubishi Electric Research Laboratories, Cambridge, MA, USA. His research interests include coherent optical transmission systems, digital coherent receiver design, coded modulation for optical communications, and digital nonlinearity mitigation. He has served as a Reviewer for several IEEE publications including IEEE Photonics Technology Letters, IEEE Journal of Selected Topics in Quantum Electronics, IEEE Communications Letters, and the IEEE/OSA Journal of Lightwave Technology. He is also serving on the Technical Program Committee for the Optical Fiber Communications (OFC)

Kieran Parsons (M'07–SM'09) received the B.Eng. and Ph.D. degrees in electronic and communications engineering from the University of Bristol, Bristol, U.K., in 1992 and 1996, respectively. During 1997–2002, he was with Nortel Networks, Ottawa, Canada, where he worked on wireless and long-haul optical communications system architecture and design. From 2004–2006, he worked on carrier-grade mesh WiFi RF system design at BelAir Networks (now part of Ericsson) and from 2006–2009 on 10-G PHY device development with Applied Micro, both in Kanata, Canada. In 2009, he joined Mitsubishi Electric Research Laboratories, Cambridge, MA, USA, where where he is currently Team Leader and Senior Principal Research Scientist. His research interests include digital signal processing and coherent optical transmission systems.

Milutin Pajovic (M'15) received the PhD degree in Electrical and Ocean Engineering from the Massachusetts Institute of Technology and Woods Hole Oceanographic Institution, in September 2014. He joined Mitsubishi Electric Research Labs (MERL) in Cambridge, MA, in September 2014, where he currently works as a Research Scientist. His main research interests lie in the areas of signal processing, statistical inference and machine learning, applied to physical layer optical and wireless communications.

Valeria Arlunno (SM'10–M'13) received the B.Sc. and M.Sc. degree in telecommunications engineering from Politecnico di Torino, Torino, Italy, respectively, in 2006 and 2009. She received her Ph.D. in Optical Communications Engineering at DTU Fotonik, Technical University of Denmark, in 2013, with a thesis on advanced equalization for digital coherent receivers. She was a Research Assistant at the Optcom Group, Politecnico di Torino in 2009 and a postdoctoral researcher at DTU Fotonik in 2013. She was at MERL as a Research Scientist from March 2014 to August 2016. She is currently with Acacia Communications Inc.